Materials Today Bio 26 (2024) 101039

Contents lists available at ScienceDirect

Materials Today Bio

journal homepage: www.journals.elsevier.com/materials-today-bio

Metal-ion-controlled hydrogel dressing with enhanced adhesive and antibacterial properties for accelerated wound healing

Zihao Shen [a], Ningyi Ma [a], Juan Xu [c,d,**], Ting Wang [a,b,*]

[a] Aulin College, Northeast Forestry University, Harbin, Heilongjiang, 150000, China
[b] College of Chemistry, Chemical Engineering and Resource Utilization, Northeast Forestry University, 26 Hexing Road, Harbin, 150040, Heilongjiang, China
[c] NHC Key Laboratory of Reproductive Health Engineering Technology Research, Haidian District, No. 12, Da Hui Si Road, Beijing, 100081, China
[d] National Research Institute for Family Planning, Haidian District, No. 12, Da Hui Si Road, Beijing, 100081, China

ARTICLE INFO

Keywords:
Hydrogel dressing
Trauma repair
Ion-control
Hyaluronic acid
Dopamine
Biodegradation

ABSTRACT

In order to improve the wound repair environment, this research has successfully developed a new multifunctional hydrogel dressing, which has strong adaptability and can accelerate wound healing. Pioneering the development of metal-ion-controlled hydrogel dressings, this research integrates dopamine and imidazole double crosslinked networks with metal-ion coordination. The resulting hydrogel dressing exhibits a notable antibacterial effect and exceptional mechanical properties, withstanding pressures of up to 12 kPa, tensions of 25 kPa, and maintaining skin adhesion at 6 kPa. Furthermore, the dressing can self-heal within only 7–8 s post-injection. Impressively, the hydrogel achieves complete biodegradation within a short timeframe (37 h). Notably, the use of various metal ions facilitates painless peeling during the degradation period, perfectly aligning with the requirements of an ideal wound dressing. This study has made significant progress in the fields of trauma repair and materials, providing strong solutions for dealing with harsh post-traumatic environments.

1. Introduction

The Bacterial infections are indeed one of the second leading causes of death worldwide, with approximately one eighth of deaths in 2019 attributed to such infections [1]. Various factors, including war injuries [2] and burns [3]. In addition, infection [4], malnutrition [5], diabetes [6], contribute to increased risks and mortality rates associated with wound infections. The delay in wound healing poses serious threats to human health [7], necessitating the development of advanced wound dressings for timely intervention [8].

In 2018, federal healthcare insurance participants reported 8.2 million cases related to wounds, with estimated medical insurance costs for acute and chronic wound care ranging from $ 28.1 billion to $ 96.8 billion [9]. These figures underscore the critical importance of infection prevention and robust wound care practices. Presently, the removal of traditional dressings can inadvertently cause secondary injuries [10], amplifying patient discomfort and diminishing treatment efficacy. Therefore, wound dressings play a pivotal role in reducing treatment costs and improving efficiency.

The advent of functional hydrogel dressings in practical medical applications has significantly elevated the quality of wound healing [11]. Studies indicate a substantial decrease in wound infection incidence from 70.1% to 26.5%, sepsis from 52.7% to 17.3% (Fig. 1A), functional impairment decreased from 82.3% to 25.1% (11,12), and the rate of post-treatment deformities from 22.5% to 13.6% (Fig. 1C). These dressings also lead to a reduction in average preoperative preparation days from 9.2 to 3.7 (Fig. 1B) and a decrease [12] in average hospital stay from 35.9 days to 17.2, showcasing their remarkable impact on critical wound treatment success rates and cost-effectiveness.

In recent years, research in this area has received widespread attention. Yang et al. [13] successfully synthesized an antibacterial hydrogel with high adhesion, utilizing the catechol group to impart

Abbreviations: **HIDs**, Hyaluronic Acid-Imidazole & Hyaluronic Acid-dopamine hydrogels; **HA-Im**, Hyaluronic Acid-Imidazole; **HA-DOPA**, Hyaluronic Acid-Dopamine; **DOPA·HCl**, Dopamine hydrochloride; **NHS**, *N*-hydroxysuccinimide; **EDC·HCl**, 1-(3-Dimethylaminopropyl)-3-ethylcarbodiimide hydrochloride; **DMF**, *N*, *N*-dimethylformamide; **DCM**, dichloromethane; **TFA**, trifluoroacetic acid; **HA**, Sodium hyaluronate; **Im**, imidazole.

* Corresponding author. Aulin College, Northeast Forestry University, Harbin, Heilongjiang, 150000, China.
** Corresponding author. NHC Key Laboratory of Reproductive Health Engineering Technology Research, Haidian District, No. 12, Da Hui Si Road, Beijing, 100081, China.
E-mail addresses: xujuan@nrifp.org.cn (J. Xu), thundersking@aliyun.com (T. Wang).

https://doi.org/10.1016/j.mtbio.2024.101039
Received 21 January 2024; Received in revised form 11 March 2024; Accepted 22 March 2024
Available online 29 March 2024

strong adhesion to the hydrogel, to impart strong adhesion to the hydrogel. Chung et al. [14] demonstrated that a hydrogel comprising dopamine and hyaluronic acid exhibits excellent adhesion. Meanwhile, Zheng et al. [15] evaluated the impact of imidazole on the mechanical strength of hydrogels. However, in current research, most of them lack controllable changes in the adhesion of such dressings during removal, which poses a risk of secondary damage. Moreover, the antibacterial ability has not been optimized, and there has been no in-depth study on its evaluation of wound repair ability.

The future emphasis in advanced hydrogel dressings research [16] lies in enhancing the functionality of the dressings to expedite wound healing [17], bolstering antibacterial safety and efficacy, and refining the mechanical properties of hydrogels. Thereafter, based on hyaluronic acid [18,19,20], this study employs a combination of imidazole derivatives [21] & dopamine [22,23] to prepare an advanced functional hydrogel dressing, utilizing various metal-ions to achieve metal-ion-control of the dressings. The hydrogel, enriched with imidazole derivatives, exhibits robust biological activity, resulting in an enhanced antibacterial effect [24,25]. Meanwhile, the presence of catechol group in dopamine-grafted hydrogel amplifies its biomineralization capability, facilitating material-mediated regulation of biological organisms. Here, hyaluronic acid-imidazole is defined as HA-Im, and hyaluronic acid-dopamine is defined as HA-DOPA. The hydrogel crosslinked by the two is abbreviated as HIDs. These impart self-healing, injectable, and biocompatible properties to the hydrogels [26]. With the aim to broaden the market for advanced wound dressings and extend the realms of theoretical research in chemistry, clinical medicine, and materials science.

2. Materials and methods

2.1. Materials

Dopamine hydrochloride (DOPA·HCl): 98% (ω), *N*-hydroxysuccinimide (NHS): 99% (ω), 1-(3-Dimethylaminopropyl)-3-ethylcarbodiimide hydrochloride (EDC·HCl): 99% (ω), *N*,*N*-dimethylformamide (DMF), dichloromethane (DCM), trifluoroacetic acid (TFA) were purchased from Aladdin (China). Sodium hyaluronate (HA), imidazole (Im), 1,6-dibromohexane, *tert*-butyl carbamate, ethyl acetate were purchased from Rhawn (China). Potassium carbonate (K_2CO_3), methanol were purchased from Meilunbio (China).

2.2. Preparation of the hyaluronic acid-imidazole & hyaluronic acid-dopamine hydrogels

2.2.1. Synthesis of tert-butyl (6-bromohexyl) carbamate

The synthesis of *Tert*-Butyl (6-bromohexyl) carbamate (*N*-Boc-BHA) represents a novel method developed by our project team. In brief, his process involves stirring an appropriate quantity of *tert*-Butyl carbamate and 1,6-Dibromohexane at room temperature. Following a day of stirring, the solution is rotated and evaporated to yield *N*-Boc-BHA.

2.2.2. Synthesis of imidazole derivatives

To synthesize Boc-protected imidazole derivatives, a mixture of 0.34 g imidazole and 0.83 g K_2CO_3 were combined with 5 mL of DMF. Subsequently, *N*-Boc-BHA was added dropwise to a beaker, and the reaction was carried out at 50 °C (700 r·min^{-1}) for 12 h. Following solvent evaporation and spin drying, the residue was treated with 15 mL of ethyl

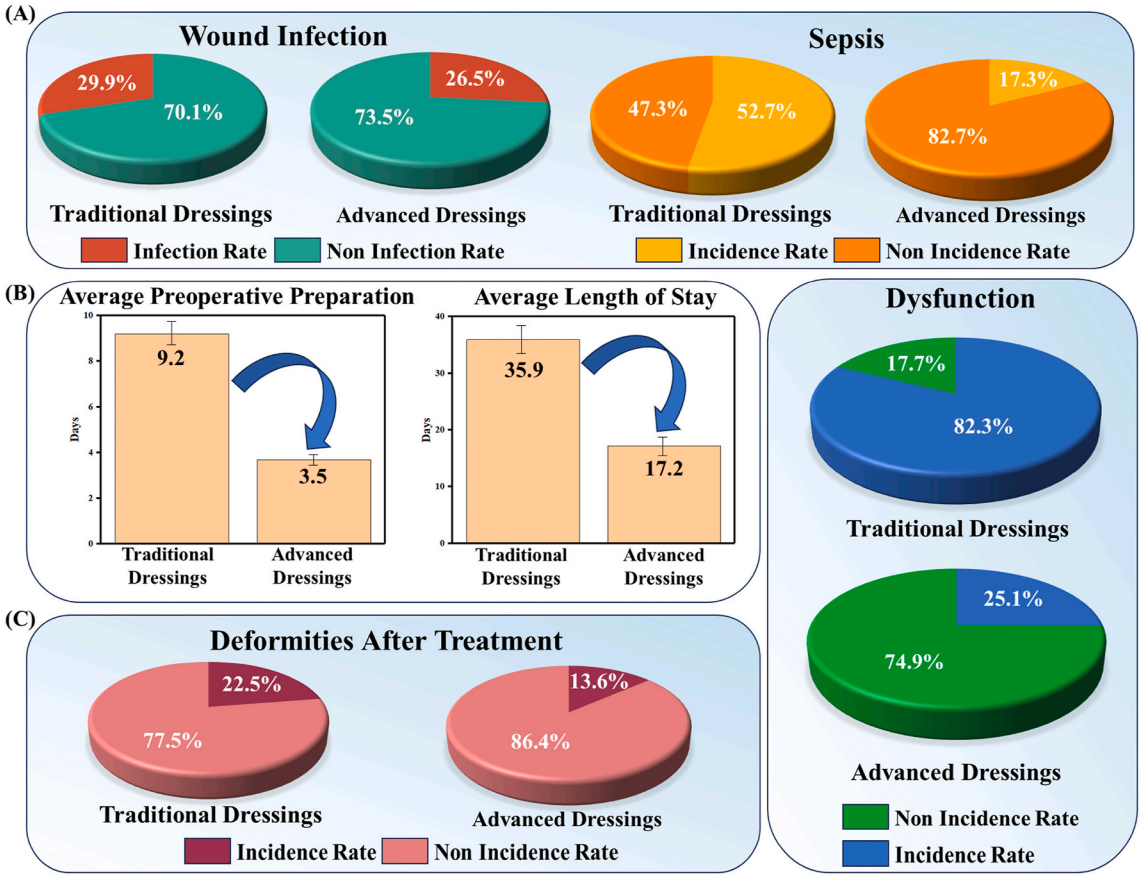

Fig. 1. Today's advanced functional dressings are an improvement in clinical medicine. (**A**) Changes in the incidence of wound infection and sepsis. (**B**) Average preoperative preparation days and average hospital stay, incidence of functional impairments, $^{**}P < 0.01$. (**C**) Changes in the incidence of post-treatment deformities between traditional and advanced.

acetate. The resulting solution underwent three extractions with 10 mL of ultrapure water, and the organic layer was collected. After drying overnight with anhydrous Na_2SO_4, the filtrate, now a light-yellow product, was obtained.

The preceding product was dissolved in 3.6 mL of dichloromethane, and 1.8 mL of trifluoroacetic acid was added, with stirring for 2 h. The solvent was then spun dry, and methanol was introduced before repeating this operation five times to yield a yellow oily product.

2.2.3. Synthesis of hyaluronic acid-dopamine, hyaluronic acid-imidazole and HIDs

Weigh 0.2 g of HA, put it into a flask, and add 9 mL of high-purity water. Stir and dissolve the HA at room temperature, adjusting the pH to 5.5 once fully dissolved. Sequentially, add 0.382 g of catalyst EDC and 0.345 g of NHS, stirring thoroughly to dissolve. Next, introduce the appropriate amount of DOPA·HCl. Apply nitrogen gas for 15 min, seal the flask, and continue to vacuum for an additional 15 min to eliminate air and prevent dopamine oxidation. Simultaneously, incorporate Fe^{3+}.

Activate the reaction in an ice bath at 4 °C for 30 min, then add an appropriate amount of Im derivative. Allow the reaction to proceed at a low temperature of 4 °C for 24 h. Following the reaction, transfer the mixture to dialysis bag (Mw = 8,000 Da) for dialysis in methanol/water ($^{V}/_{V}$ = 1:1) for 1 day, followed by dialysis in water for 2 days. Complete the process with freeze drying to ultimately obtain the target hydrogel (HIDs) product.

2.2.4. Measurements

FT-IR measurements were performed using an FT-IR Spectrometer (Agilent, USA). Additionally, the elemental analysis was conducted to characterize the compounds, utilizing an Organic elemental analyzer vario MACRO cube CHNS (Elementar, Germany). The morphological distribution of the hydrogel was observed by SEM (Hitachi, Japan). This approach was employed to provide support and confirmation of the composition and structure.

2.2.5. Rheological characteristics

For rheological testing, detection, and analysis, the AR-G2 Rheometer (TA Instruments, USA) was used. To characterize the linear and nonlinear viscoelastic properties of chemically crosslinked hydrogels [27], all hydrogels were tested separately at 25 °C. Oscillatory shear measurements under a series of strain amplitudes were conducted. The initial thickness of the hydrogel samples utilized for frequency sweep, tensile and compression tests ranged from 5 to 8 mm.

2.2.6. Healing capability and injectable properties

In the optical visualization experiment at room temperature, delicately incise the hydrogel in the middle and reposition the two parts of the hydrogel together for observation. The self-healing of the hydrogel was recorded and observed with the DSLR camera (Nikon, Japan). Concurrently, the injectability of HIDs was tested by injecting a syringe into molds and inscribing words on a room temperature platform. The experimental phenomena were recorded in real-time using an action camera (DJI, China).

2.2.7. Mechanical characterization and metal-ion responsiveness properties

The universal testing apparatus (Shimadzu, Japan) is used to characterize the mechanical properties through tensile testing at a rate of 4 mm min^{-1} and a compression testing at a rate of 1 mm min^{-1} at room temperature. The adhesion of hydrogels was evaluated by tensile adhesion test. In this test, a hydrogel sample (20 mm × 20 mm × 2 mm) was placed between two pigskins, sourced from 7-months old boars. A weight was applied to the overlapping position of the pigskins for 5 min, followed by a uniaxial tensile test using a universal testing machine at a rate of 5 mm min^{-1}. This process was conducted to determine the adhesion strength of the hydrogel in a skin application. The metal coordination in the hydrogel was confirmed by EDS (Hitachi, Japan) detection and analysis.

2.2.8. Evaluation of antibacterial activity and assessment of cytotoxicity

The Oxford Cups were used to conduct antibacterial performance testing using the inhibition zone method, which is highly intuitive. The testing procedure involves the following steps: (1) Preparation of test drug mother liquor. (2) Activation of the culture test strain by scribing (*Escherichia coli & Staphylococcus aureus etc.*). (3) Expansion of the cultivation of test strains in liquid medium under suitable conditions. (4) Preparation of a plate containing bacteria culture medium (Radius = 30 mm), placement of a sterile Oxford cup, and subsequent injection or non-injection of hyaluronic acid hydrogel and HIDs hydrogel, respectively. (5) After appropriate cultivation time, analyze the radius (mm) of the antibacterial band to evaluate its antibacterial ability.

Where the absolute difference between the two independent determination results obtained under repeated conditions should not exceed 15% of the arithmetic mean, and it can be considered that the antibacterial test conclusion is valid.

After activation, the test strains were inoculated onto nutrient agar plates and cultured at 36 °C ± 1 °C for 24 h until clear colonies appeared. Take 3 colonies and disperse them in TSB liquid culture medium to prepare a bacterial suspension. Adjust the concentration of the bacterial suspension to 1.5 × 10^8 CFU·mL^{-1}. Add HIDs test samples to TSB liquid culture medium and prepare TSB liquid culture medium with concentrations of 0.1%, 0.3%, 0.6%, 0.9%, 1.2%, 1.5%, 1.8%, 2.1%, and 2.4%, respectively. Take 30 μL bacterial suspension was inoculated into TSB medium containing the test sample and placed in a fully automatic growth curve analyzer (Bioscreen, Finland). The suspension was incubated at 37 °C for 48 h, and the turbidity value was measured every 3 h. The minimum inhibitory concentration (MIC) is the minimum drug concentration at which HIDs can completely inhibit bacterial growth.

To determine the cytotoxicity of the relevant hydrogels, sterilized samples were incubated at 37 °C for 24 h. After removing the hydrogel, add 200 μL the suspension about clone 929 (L-929 cell) was inoculated into a 96-well plate and cultured at 37 °C for 1 day. The extract was removed and 10% was added to MTT solution. Incubate L-929 cells in a suitable environment (37 °C, 5% CO_2) for 4 h. Then dissolve it in dimethyl sulfoxide. Read the optical density at 568 nm.

Meanwhile, the L-929 cells were inoculated into fresh culture medium under the same inoculation conditions. Calculate the significance between the means, where a probability value $^*P < 0.05$ is considered significant (n = 12).

2.2.9. Therapeutic evaluation using a full-thickness injury animal model

The treatment experiment on the full-thickness injury animal model received approved from the College of Chemistry, Chemical Engineering and Resource Utilization, Northeast Forestry University (Approval No. 2022082609). To further evaluate the efficacy of the hydrogel dressing in wound healing, wounds of a similar degree were created on the backs of mice using a high-temperature soldering iron. Wounds of a similar degree were created on the backs of mice using a high-temperature soldering iron. Following the initial treatment of the wound with physiological saline, the experimental group received treatment with HIDs, while the control group was treated with medical gauze. Ongoing observation were made on the physiological and wound healing status of mice, with records kept. Meanwhile, observations were made on the organs of the experimental mice to evaluate the potential toxic effects of the chemicals and determine their toxicity. Use the curve tools in Origin software to simulate the wound healing process. The wound healing process was simulated using curve tools in Origin software, and the area of unhealed wounds was measured using ImageJ software. The wound healing rate was calculated using a specific equation (1):

$$\text{Wound closure}\ (\%) = \frac{A_0\text{-}A_t}{A_0} \times 100 \quad (1)$$

where the wound areas on day 0 and day t were A_0 (cm^2) and A_t (cm^2). Use Image to calculate the irregular area of the wound.

In addition, on the 12th day, mice from both the experimental and control groups were euthanized, and tissue samples from the surrounding areas were collected and organ slices. These samples were fixed in 4% paraformaldehyde for 48 h, embedded in paraffin, sliced, and stained with Hematoxylin Eosin (H&E) and Masson trichrome for histological analysis.

2.2.10. Statistical analysis

Employ statistics methods to compare group differences and evaluate their statistical significance. Utilize mean standard deviation for the analysis of data collected from distinct parallel surveys. Perform statistical analysis using Office and Origin software. The significance level is set at $^*P < 0.05$, indicating statistical significance $^{**}P < 0.01$ denotes high statistical significance $^{***}P < 0.001$ signifies the highest level of statistical significance.

3. Results

3.1. Structural analysis of HIDs hydrogel

This stepwise polymerization scheme utilizes amide bonds to form two types of hyperbranched hyaluronic acids: DOPA functionalized hyperbranched HA and Im functionalized branched HA. Simultaneously, we employ metal coordination to alter its mechanical strength and achieve controllable mechanical performance. The detailed internal chemical structure of the hydrogel dressing is shown in Fig. 2B.

For the hydrogel, HA serves as the foundation. Both Im and Fe^{3+} are incorporated to endow the hydrogel with outstanding antibacterial properties. Furthermore, the infusion of dopamine-modified HA augments the mechanical strength and wound healing efficacy of the said hydrogel.

Regarding the architecture of the hydrogel, we have elected to employ a double network construction strategy. This involves the incorporation of HA and Im derivatives to establish a durable, cross-linked network (HA-Im). The secondary network is realized through the grafting reaction between DOPA and HA, leading to the formation of HA-DOPA. These two networks are intertwined through metal coordination with Fe^{3+} to create reversible cross-links. Subsequently, we will delve into the unique function provided by the spray application of Cu^{2+} - enabling the gel to peel off painlessly. An examination of the SEM image depicted in Fig. 2C indicates that the HIDs possess a spatial network structure that is denser compared to the HA found in the unprocessed material. This enhanced structure boosts its swelling capacity, facilitating the penetration of the corresponding solution through the network [28].

According to the infrared spectrum, HA-DOPA has a = C–H absorption frequency around 3100-3000 cm^{-1} on the aromatic ring, in contrast to HA and HA-Im, showing three weaker peaks. The skeletal stretching vibration of the C═C aromatic ring normally has four bands, approximately 1600, 1580, 1500 and 1450 cm^{-1}. At the same time, the series of minor peaks around 2000-1700 cm^{-1} is presumed to represent the overtone peaks of the aromatic C–H bending vibrations of benzene ring derivatives. It has been demonstrated that DOPA has been successfully grafted in this condition. At the same time, the characteristic peak of 1601 cm^{-1} in HA-Im is also favorable evidence for the grafting of imidazole derivatives onto HA. The FTIR spectrum of HIDs hydrogel is shown in Fig. 2A, revealing distinctive features. Notably, the absorption peak in the range of 3500 and 3200 cm^{-1} is associated with –OH, while the absorption peak at 1644 cm^{-1} corresponds C═C, and the peak at 1203 cm^{-1} is linked to C–N. These findings provide evidence that Im derivatives and dopamine have been grafted onto HA, resulting in the formation of the observed products.

For CHN analysis, the sample is introduced into the equipment using a silver crucible, and combustion is facilitated by injecting oxygen using inert gas [29]. This test uses a standard sample of sulfanilic acid within the range of 0.15–0.50 mg for calibration (Fig. 2B). Table 1's comparison with HA reveals that DOPA-grafted and Im-grafted hydrogels possess a higher carbon content. At the same time, both HA-Im and HIDs showed a significantly higher nitrogen content compared to HA, which serves as crucial evidence of successful Im grafting. Furthermore, the successful attachment of DOPA and Im onto HA is confirmed by their unique C/N ratios. The C/H ratio of HIDs is measured at 8.29%, closely aligning with the theoretical value of 8.32%. These results affirm the successful modification of HA through the process of grafting DOPA and Im into the hydrogel.

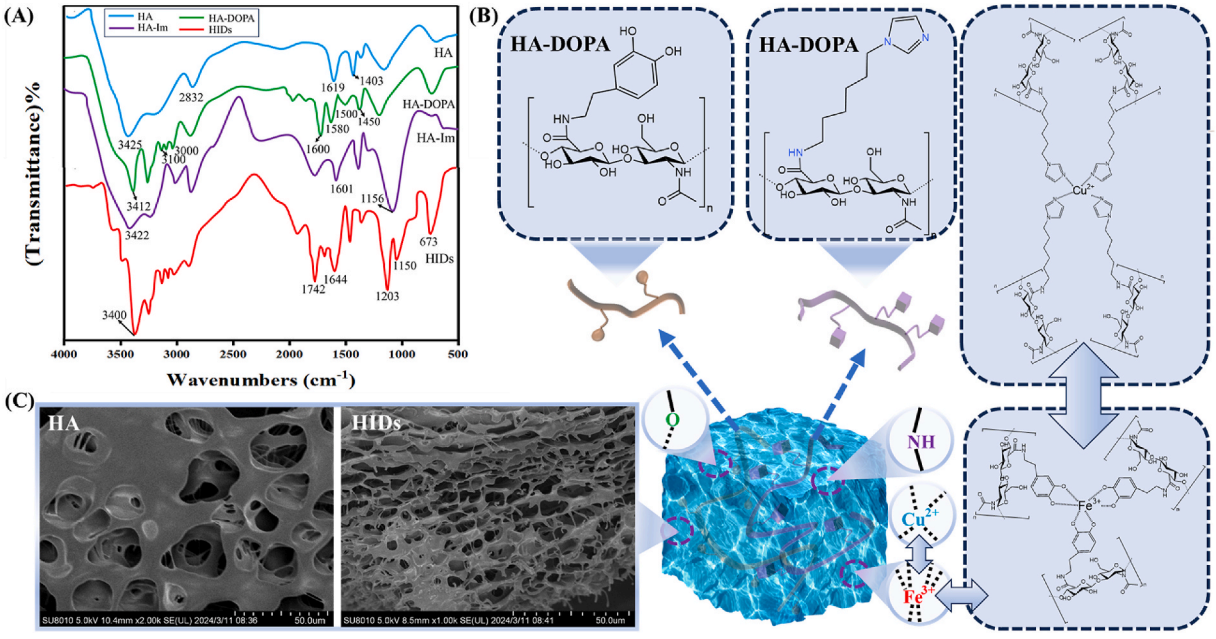

Fig. 2. Structure and composition characterization of hydrogels. (**A**) The FT-IR spectra of HA, HA-DOPA, HA-Im, HIDs. (**B**)Schematic diagram of structure and composition of HIDs hydrogel. (**C**) The SEM images of hydrogel (HA & HIDs).

Table 1
The sample data in CHN analysis.

Group	Element	HA	HA-Im	HA-DOPA	HIDs
Theoretical Value	**C**	44.32%	50.40%	51.36%	50.89%
Actual Value		44.26%	50.43%	51.10%	50.23%
Theoretical Value	**H**	3.69%	6.40%	5.84%	6.11%
Actual Value		3.74%	6.47%	5.79%	6.16%
Theoretical Value	**O**	46.44%	32.00%	37.35%	34.71%
Actual Value		46.78%	32.12%	37.21%	34.62%
Theoretical Value	**N**	5.54%	11.20%	5.45%	8.28%
Actual Value		5.50%	11.15%	5.51%	8.31%
Theoretical Value	**C/H Ratio**	12.01%	4.50%	8.79%	8.32%
Actual Value		12.13%	4.56%	8.82%	8.29%
Theoretical Value	**C/N Ratio**	8.00%	7.86%	5.84%	6.15%
Actual Value		8.04%	7.74%	5.32%	6.49%

3.2. Rheological analysis

The gelation time of HIDS and ha hydrogels was evaluated (Fig. 3A). Over time, the values of G′ and G″ for HIDS gradually increased. The sol-gel transition initiated in 22 s and reached equilibrium within 28 s, indicating completely crosslinking (Fig. 3C). As the temperature is tested within the temperature range of the normal environment, the modulus of gel is almost stable, reflecting that the HIDs hydrogel can maintain the best lasting mechanical properties compared with other control groups in clinical application (Fig. 3D). Notably, the gelling time of HIDs was shorter than that of HA. Subsequently, frequency scanning was carried out on the hydrogel, revealing stable values of G′ and G″ with minimal fluctuation within the dynamic frequency range (Fig. 3E).

Simultaneously, the hydrogel exhibited a linear viscoelastic zone and excellent shear resistance within a 0%–100% (Fig. 3F). This observation indicates the integration of the crosslinked structure of the hydrogel, forming a stable three-dimensional polymer network structure.

In the angular frequency scanning range of 1–100 rad s^{-1}, the value of G′ is consistently exceeded G″ for HIDs, HA, HA-DOPA and HA-Im hydrogels (Fig. 3E). This indicates the successful formation of elastic solid hydrogels [30]. Additionally, due to the change in the chemical cross-linking network, the modulus of HIDs is significantly greater than that of the other three hydrogel products.

3.3. Mechanical properties of HIDs

The mechanical properties of the hydrogel were measured by compression and tensile tests (Fig. 3B). Uniform tensile and compressive force to the hydrogel samples, and resulting deformations and modulus were measured modulus (Pa) and strain (%). Tensile stress-strain curves (Fig. 3F) and compressive stress-strain curves (Fig. 3G) for each group were obtained. The results show that HIDs hydrogels can withstand up to 90% strain without cracking (Fig. 3G). This suggests that the addition of DOPA and Im enhances the crosslink density of the double crosslinked structure formed by the HIDs hydrogel compared to a single crosslinked structure. This improvement effectively addresses the issue of weak mechanical properties in hyaluronic acid hydrogel.

Additionally, the hydrogel exhibits robust adhesion to biological tissues such as skin and liver, sourced from 7-months old boars (Fig. 4A). The strong adhesion between wound dressings and skin is particularly advantageous for widespread application. The primary contributor to adhesion force is the van der Waals force between the wound dressing and the skin. In the pig skin adhesion test, we observed that the adhesion strength of HIDs-Cu^{2+} on the skin can even reach 6 kPa (Fig. 3H), which is sufficient to meet their needs for wound treatment. As illustrated in Fig. 4B, the HIDs hydrogel adheres well to the hand and remains secure during frequent limb movements. The hydrogel's strong adhesive force, coupled with its ability to extend or contract with finger bending, enhances its efficacy in wound healing [31]. These observations underscore the hydrogel dressing's effectiveness in clinical wound care applications.

Another crucial aspect of the investigation involves examining the impact of incorporating various metal ions, on adhesion strength. Cu^{2+} are an important factor in wound healing, as well as in angiogenesis and induction of vascular endothelial growth factor. Local release of Cu^{2+}

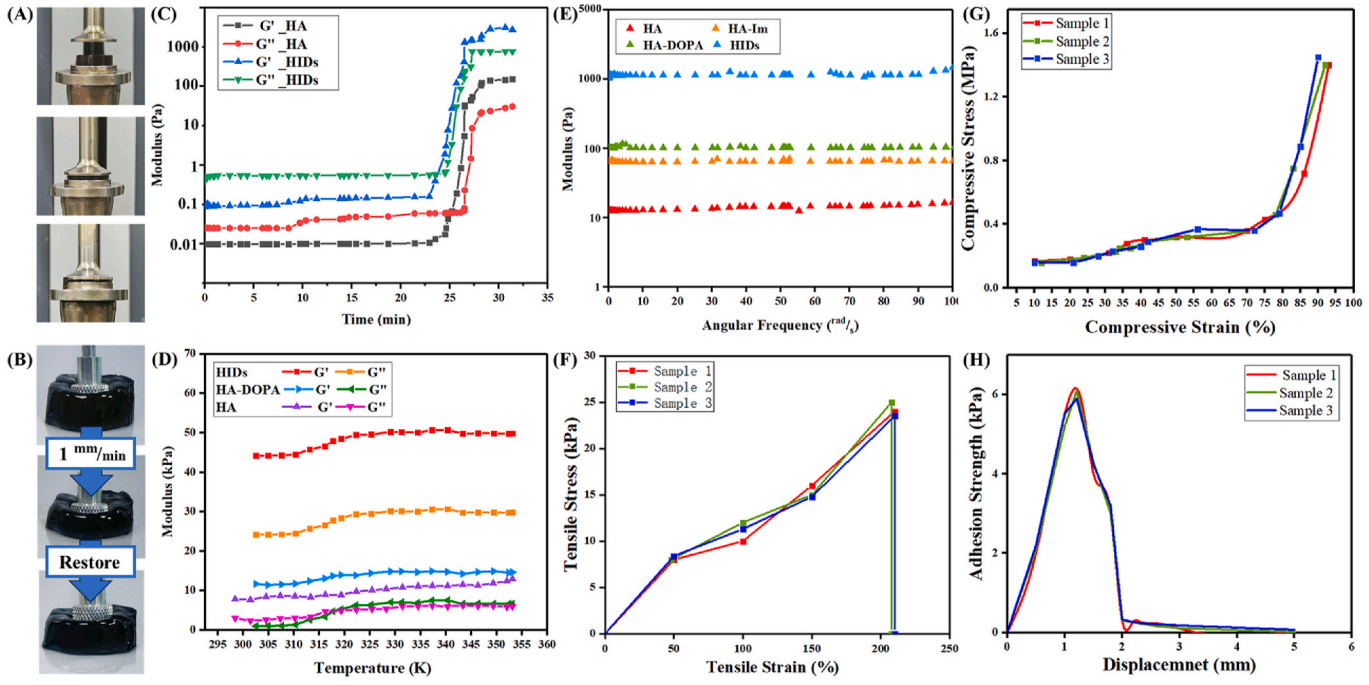

Fig. 3. Test the characterization and rheological properties of HIDs. (**A**) AR-G2 Rheometer was used to test the rheological properties of HIDs hydrogel. (**B**) The universal testing apparatus is used to test the mechanical properties of HIDS hydrogel samples. (**C**) Gelation process of hydrogels (HA and HIDs). ***$P < 0.001$. (**D**) The temperature (K) scanning was performed on the hydrogel. ***$P < 0.001$. (**E**) The hydrogel samples were frequency scanned. ***$P < 0.001$. (**F**) Tensile stress-strain curves of HIDs. ***$P < 0.001$. (**G**) Compressive stress-strain curves of HIDs. (**H**) Adhesion mechanical curves for pigskins. ***$P < 0.001$.

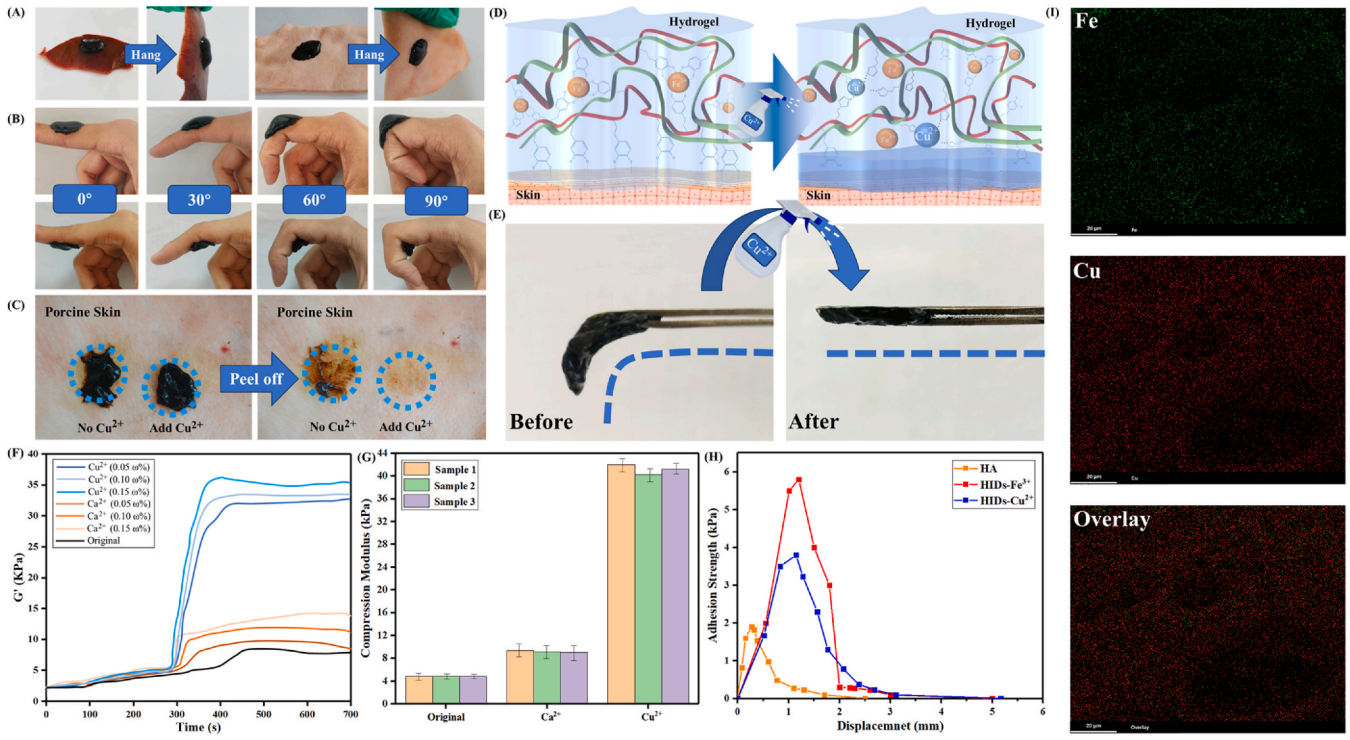

Fig. 4. Test the adhesion and controllable peeling ability of HIDs. (**A**) Adhesion testing on animal organs. (**B**) The hydrogel is tested on the outside and inside of the fingers. To get the statistical data, at least 5 duplicate samples were used. To get the statistical data, at least 5 duplicate samples were used. (**C**) Controllable peeling of HIDs hydrogel on pig skin surface. (**D**) Schematic diagram of HIDs hydrogel controllable adhesion principle. (**E**) Rheological analysis of HIDs hydrogel with various metal ions added within 600 s. (**F**) Modulus of HIDs hydrogels after encountering different concentrations and different kinds of metal ions for 8 min. (**G**) Compressive modulus of HIDs-Cu^{2+} hydrogel after adding Ca^{2+} and Cu^{2+} for 1 h (Number of parallel experimental samples = 3). ***$P < 0.001$. (**H**) Adhesion performance curve of HIDs hydrogel crosslinked by different metal ions and HA hydrogel on pigskin. ***$P < 0.001$. (**I**) The EDS testing on HIDs-Cu^{2+} of elements (Cu and Fe).

has been shown to facilitate wound healing [32]. At the same time, by adding different metal ions (such as Cu^{2+}, Ca^{2+}) to peel off pig skin (from 7-months old boar) to evaluate the adhesive strength, the changes caused by hydrogel dressing were visually captured (Fig. 4G) in a long time. In order to achieve the optimal effect of controllable stripping, as shown in Fig. 4F, by adding Cu^{2+} and Ca^{2+} for comparison, the G′ of HIDs hydrogel caused by Cu^{2+} increases significantly and immediately, while the modulus change caused by Ca^{2+} is very insignificant, and the effect of Ca^{2+} is far less than that of Cu^{2+}. Meanwhile, through EDS testing to detect Cu and Fe elements in HIDs-Cu^{2+} (Fig. 4I), we found that after spraying Cu^{2+}, Cu^{2+} quickly competes with Fe^{3+} and occupies most of the coordination sites, which is the main reason for the change in its adhesive strength. As the concentration of Cu^{2+} sprayed increases, the adhesion of the hydrogel correspondingly decreases, facilitating easier and painless peeling. Given that the maximum daily intake of Cu^{2+} permissible in the human body is 0.5 mg kg^{-1} d^{-1} [33], for an average human body weight of 50 kg [34], the daily dosage should not exceed 25 mg. However, this hydrogel achieves the targeted detachment at a usage of just 5 mg, rendering safety concerns negligible.

As shown in Fig. 4C, in the presence of Fe^{3+}, it is observed that the adhesion strength of HIDs hydrogel is very strong, and it is difficult to completely peel off. However, after 8 min of Cu^{2+} reaction, the adhesion strength sharply decreased (Fig. 4H). The hydrogel compounded with Cu^{2+} could be easily peeled off from pigskin, with the residual amount being nearly negligible (Fig. 4C). As shown in Fig. 4E, it illustrates that the HIDs-Fe^{3+} hydrogel, naturally sagging under gravity, could overcome its own weight and straighten horizontally within 2 min due to the rapid increase in mechanical strength after Cu^{2+} spraying. We associate this occurrence with shifts in the composite of metal-ions, in which the coordination ability of Cu^{2+} exceeds that of Fe^{3+} [35]. This discrepancy results in alterations to the degree of internal cross-linking. Consequently, a new hydration layer materializes between the hydrogel and the wound. This new layer diminishes the intimate contact between the polymer and the wound surface, thereby nullifying the bidentate hydrogen bond formed between DOPA and the skin. Consequently, with the disintegration of the hydrogen bond, the adhesion strength of the hydrogel dissipates rapidly.

In summary, HIDs hydrogels exhibit excellent rheological and adhesive properties for the skin and demonstrate controllable peeling of dressings after Cu^{2+} application. Compared to HIDs-Fe^{3+}, HIDs-Cu^{2+} has a reduced adhesive strength, which makes it difficult to replace dressings, reduces pain during the removal process. The HIDs hydrogel will be changed by complexing metal ions with the water entering (Fig. 4D). When the new hydration layer is formed, the real contact area between the hydrogel and the matrix is greatly reduced, which will greatly weaken the close contact between the adhesive polymer and the tissue surface, and eliminate the influence of the hydrogen bond between DOPA and the surface. Thus, achieving painless dissection, avoids secondary damage, and thus improves debridement efficiency and accelerates wound healing speed.

The biodegradability of hydrogel dressings is expected to maintain its function, especially its mechanical integrity, within the required service life. The self-degradation [17,36] of HIDs hydrogel (Fig. 5B) includes (i) hydrogels that disintegrate along the main chain, (ii) hydrogels with pyrolysis crosslinks, and (iii) hydrogels with degradable side chains. Hydrogels exhibit various changes in mechanical properties at different degradation stages.

The natural degradation experiment confirmed that HIDs hydrogel showed excellent self-degradation rate at normal temperature and pressure (Fig. 5A). Notably, *in vitro,* the residual mass of HIDs hydrogel after 24 h is only approximately 25%. In comparison with other control groups, this represents a significant improvement in the degradation

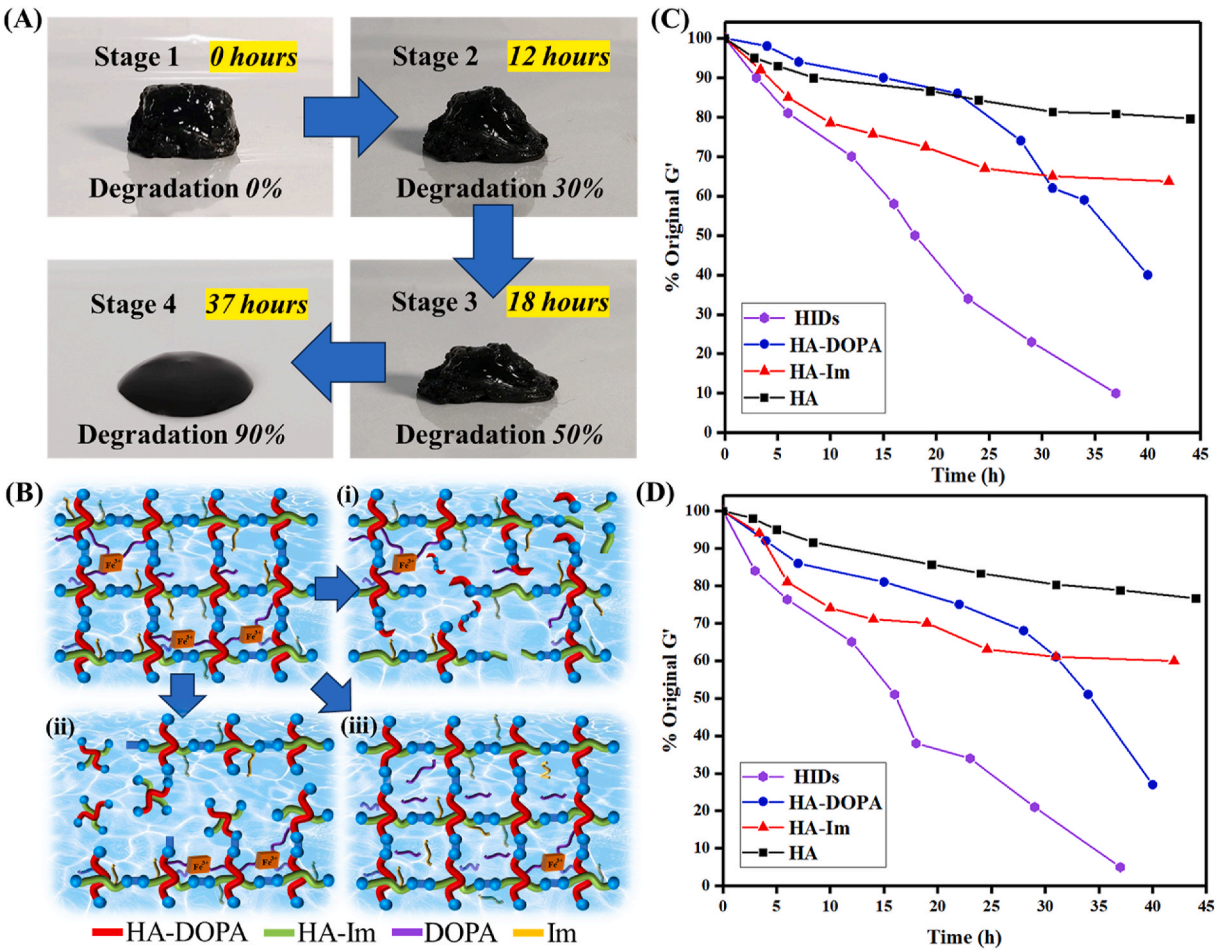

Fig. 5. Analyze the degradability of HIDs. (**A**) Degradation process of HIDs hydrogel dressing. (**B**) Schematic diagram of degradation principle of HIDs hydrogel. (**C**) Diagram of degradation degree and time of hydrogel (HIDs, HA-DOPA, HA-Im and HA) *in vitro*. (**D**) Diagram of degradation degree and time of hydrogel (HIDs, HA-DOPA, HA-Im and HA) *in vivo*.

rate. Specifically, the residual mass of HA hydrogel and HA-DOPA hydrogel at the 24th hour is around 90%, and that of HA-Im hydrogel is approximately 70% (Fig. 5C). *In vivo* experiments (Fig. 5D), HIDs have a faster degradation rate compared to other groups, with only about 4% remaining after about 36 h, even faster than *in vitro* degradation. These experimental findings provide favorable evidence for the effective self-degradation of HIDs hydrogel dressing in clinical application.

3.4. Self-healing and injectability

As demonstrated in Fig. 6B, the hydrogel can be extruded through a needle and shaped as required, showcasing its high plasticity and ability to fill uneven wounds. The adaptability of hydrogel dressings to complex-shaped wounds is crucial for their efficacy in clinical applications [37].

To evaluate the adaptability of HIDs hydrogels, injections into molds of various shapes were performed. After being placed at room temperature and under pressure for 7 s, it reconstructs into a complete hydrogel similar in shape to animals and humans. In the injection experiment, HIDs hydrogel was easily injected through a *22 G* needle (Fig. 6B) and could be successfully shaped according to specific requirements, emphasizing its versatility and applicability in diverse clinical scenarios.

In addition, the self-healing ability of HIDs hydrogels was evaluated by visual methods [38,39]. When a round HIDs hydrogel is cut into two halves under normal temperature and pressure, the two pieces of the cut semi-circular hydrogel demonstrate remarkable self-healing within just 7 s (Fig. 6C), forming a new flawless hydrogel (Fig. 6A). Notably, this self-healing occurs effortlessly without external force. The recovered hydrogel dressing still has excellent toughness and elasticity (Fig. 6D). These findings indicate that HIDs hydrogels have excellent injectability and self-healing properties due to the good remodeling ability of high dynamic hydrogel networks.

3.5. Evaluation of antibacterial activity and assessment of cytotoxicity

As is well known, biobased polymers have active functional groups such as –OH, $–NH_2$, –COOH on the molecular chain, which can form physical or chemical interactions with antibacterial agents, so that the prepared hydrogel has antibacterial properties [40]. The antimicrobial efficacy of the hydrogel is predominantly associated with imidazole. It selectively inhibits the fungal cytochrome P-450 dependent 14-α-Demethylase [41], leading to the build-up of 14-α-Methyl sterol. This prevents the synthesis of ergosterol on the cell membrane, effectively altering its permeability. Owing to this, the fungi ultimately perish due to the depletion of vital intracellular substances.

By using the bacterial growth curve method, the hydrogel's antibacterial characteristics were further investigated. The results are depicted in Fig. 7A and B. First of all, the experimental results found that the control group without hydrogel dressing had almost no antibacterial effect and almost no antibacterial circle. However, the study found that there was a slight bacteriostatic zone around the HA hydrogel (*Escherichia coli* 4.02 ± 0.10 mm, *Staphylococcus aureus* 6.07 ± 0.14 mm). Due to their radii being less than 5 mm and less than 7 mm respectively, they belong to moderate and low antibacterial properties [42]. On the other

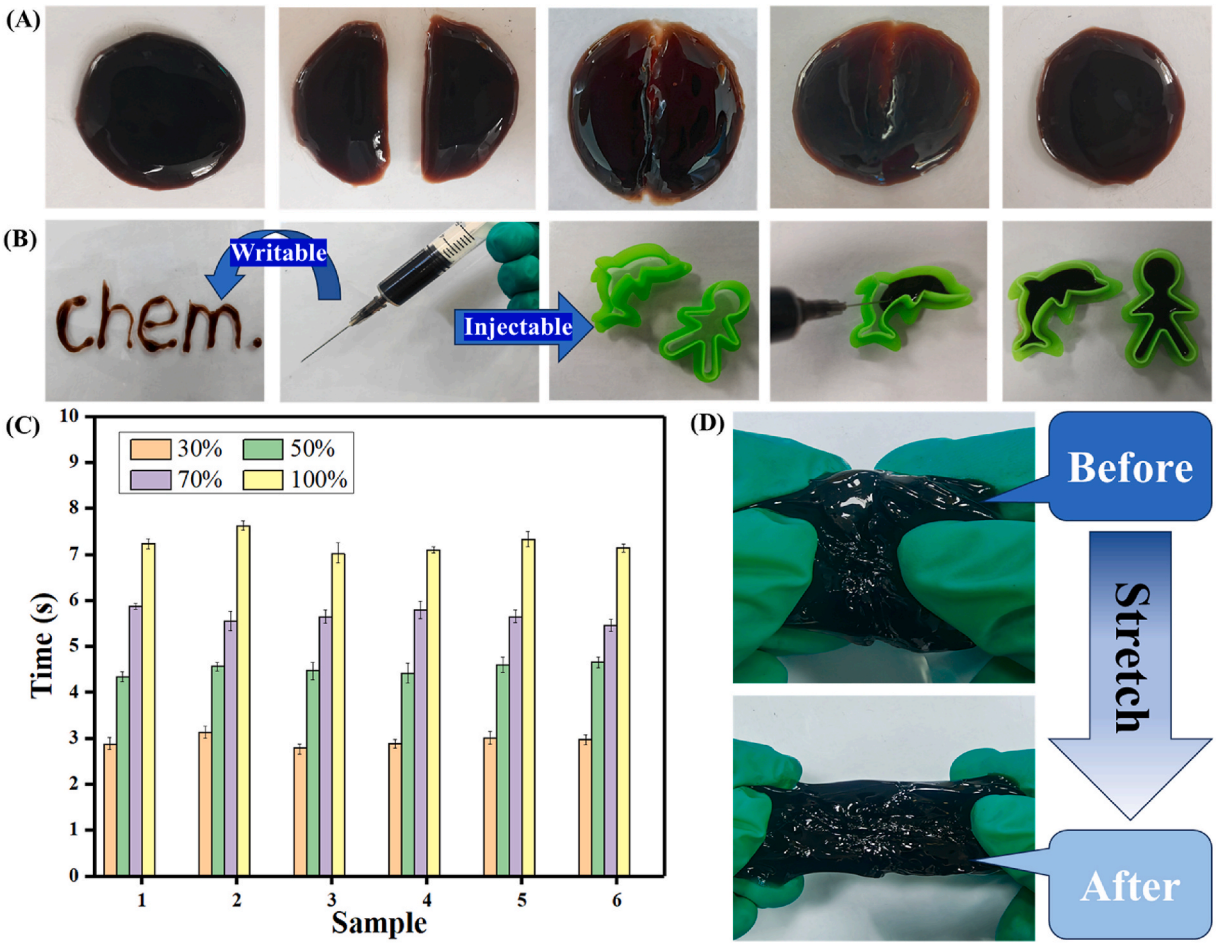

Fig. 6. Self-healing and injectability testing of HIDs. (**A**) The photographs of hydrogel self-healing process. (**B**) Macroscopic evaluation of injectability of hydrogels. (**C**) Statistical chart of time and self-healing of HIDs hydrogels in 6 groups. (**D**) After self-healing, the macroscopic diagram of strength and toughness of HIDs hydrogel dressing.

hand, HIDS hydrogel has a much better inhibitory effect on *Escherichia coli* (Fig. 7C) and *Staphylococcus aureus* (Fig. 7D), both reaching 12.01 ± 0.12 mm. Due to their radii being all greater than 10 mm, it proves that HIDs have extremely strong antibacterial properties [43]. On the other hand, based on the significant decrease in the number of the two bacteria shown in Fig. 7H and I after using HIDs, we can also visually demonstrate their excellent antibacterial properties. According to the test results shown in Fig. 7E and F, the minimum inhibitory concentrations of HIDs on *Escherichia coli* are all 2.1%, and the minimum inhibitory concentrations on *Staphylococcus aureus* are all 1.8%; When the concentration of the hydrogel is 2.4%, the antibacterial rate against *Escherichia coli* and *Staphylococcus aureus* is close to 100%.

HIDs hydrogels were evaluated by using hydrogel extracts for NCTC clone 929 (L-929 cell) culture. As shown in Fig. 7G, compared with the blank control, the optical density (OD) value at 568 nm of the HIDs hydrogel is statistically different to some extent ($^*P < 0.05$), but they still reach 85%. In adherence to the guidelines stipulated for the biological evaluation of medical devices (ISO 10993-5:2009, IDT) [44], scenarios requiring a decrease in cell viability exceeding 30% are deemed to represent cytotoxic effects. This highlights that HA exhibits no cytotoxicity towards L-929 cells. Furthermore, our results also confirm that the HIDs hydrogel displayed no signs of cytotoxicity.

3.6. Healing research

The results were compared with those of bacterial infected wounds bandaged without hydrogel dressing and with HA. The progression of wound healing in each group on treatment days 2, 6, 8, and 10 is depicted in Fig. 8B. As shown in Fig. 8A, the wounds of mice were regularly photographed and monitored within 0–10 days. After healing the wound for 6 days, the HIDs group gradually outperformed the control group, and on the 8th day of HIDs, significant epidermal regeneration was observed compared to other groups. After 10 days of treatment, compared with the control group and HA group, the HIDs group showed better wound healing characteristics, almost complete healing, and new hair growth, while the other groups still showed open wounds. This directly proves that HIDs exhibits the best wound regeneration effect among all groups. Simultaneously, sections of organs (including heart, liver, spleen, lungs, and kidneys) of mice treated with HIDs were tested (Fig. 8F). The cells in the tissue slices were intact and showed no cytotoxicity or tissue damage, proving that HIDs have wound therapeutic effects while not causing damage to other tissues and organs in the body.

Given that HA at a trauma site can effectively regulate inflammatory cells and fibroblast's movements, trigger pro-inflammatory cytokines synthesis, and assist in the phagocytosis of invading microorganisms [45,46], HA plays a crucial role in anti-inflammatory responses. These processes contribute to the notable absence of inflammation or infection at the wound site throughout the treatment, as depicted in Fig. 8A and B.

The quantitative analysis of the wound area throughout the entire skin wound repair process (Fig. 8C) showed that on the 10th day, compared with other groups, the healing rate using HIDs was 99% (about 0.02 cm^2) (Table 2), showing a significant difference, further indicating that HIDs are an excellent wound repair platform. In addition,

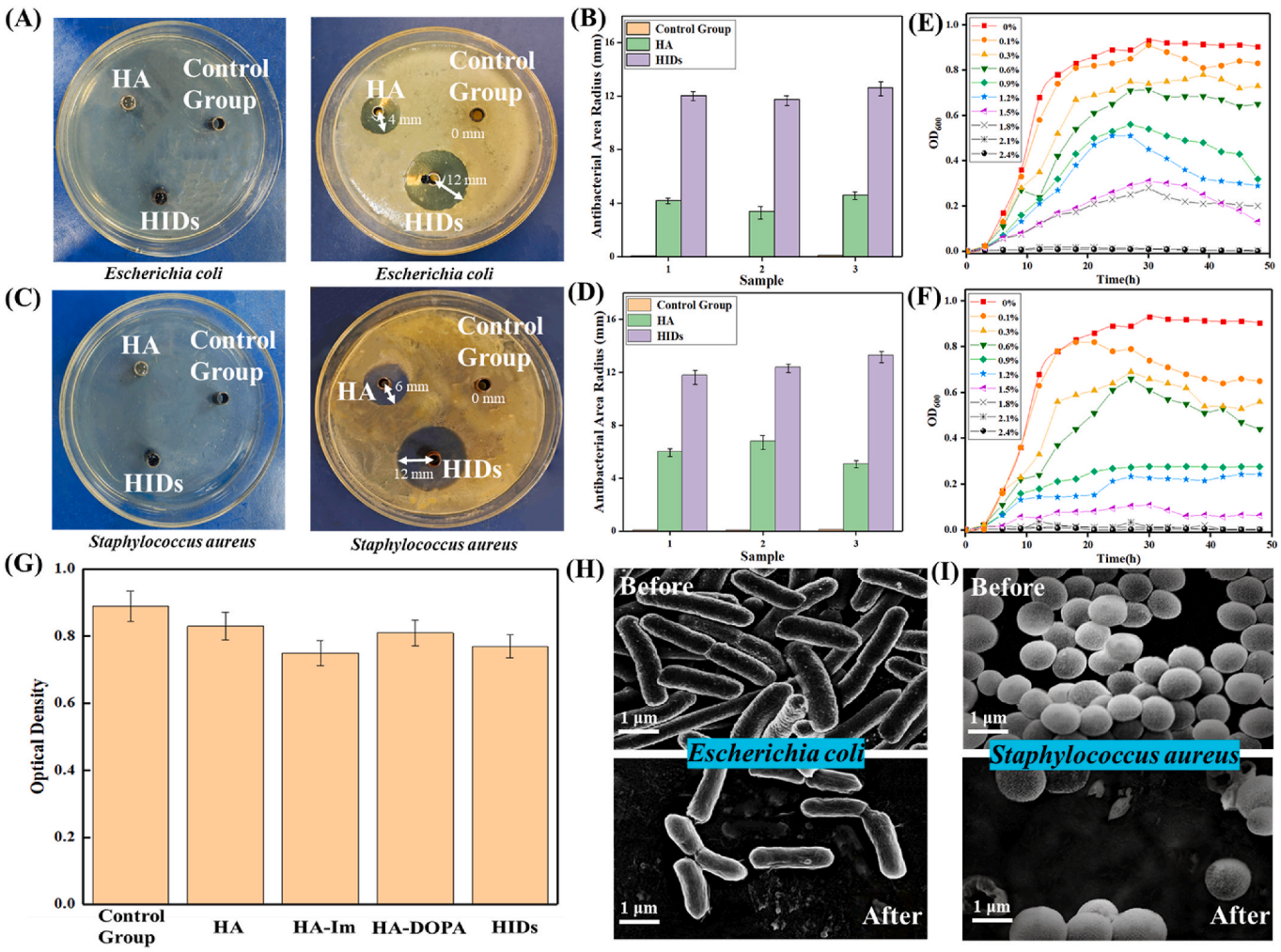

Fig. 7. Analyze the antibacterial activity & cytotoxicity assays of HIDs. (**A**) The antibacterial effect of the hydrogel group (HA, HIDs) and control group on *Escherichia coli*. (**B**) The antibacterial radius of *Escherichia coli* against the control group and various experimental groupings. (**C**) The antibacterial effect of the hydrogel group (HA, HIDs) and control group against *Staphylococcus aureus*. (**D**) The antibacterial radius of *Staphylococcus aureus* against the control group and various experimental groupings. (**E**) Determination of the minimum inhibitory concentration of HIDs on *Escherichia coli*. (**F**) Determination of the minimum inhibitory concentration of HIDs on *Staphylococcus aureus*. (**G**) Cytotoxicity assays of these hydrogels (HA, HA-Im, HA-DOPA and HIDs), $*P < 0.05$ when compared to the control group of indirect cytotoxicity. SEM images of (**H**) *Escherichia coli* and (I) *Staphylococcus aureus* before and after the inhibition zone method experiment.

the healing rate in the HA group (72%) was also significantly different from that in the control group (50%), which proved that the presence of dopamine in HIDs endowed the ability to enhance cell metabolism, stimulate collagen production, cooperate with imidazole to effectively resist bacteria, reduce inflammation and actively promote wound healing.

To further evaluate the therapeutic effect and regenerated skin quality, histological analysis was used. In H&E staining [47], hematoxylin staining solution can dye the chromatin in the nucleus and nucleic acids in the cytoplasm blue or purple, while eosin staining solution can dye them pink. The classic method in Masson trichrome's connective tissue staining [48] is the authoritative and classic technique for collagen fiber staining. The wound tissue on day 2 and day 6 showed that the multifunctional HIDs hydrogel could reduce the bacterial induced inflammatory reaction and promote the inflammatory recovery. After H&E staining, as shown in Fig. 8D, a new layer of epidermis was observed covering all wound tissues. During the wound healing process, the thickness of granulation tissue and skin appendages in HIDs was better than that in the control group, confirming that HIDs has a good wound repair effect. The results are consistent with the previous Fig. 8A and C, and are consistent with the Masson trichrome (Fig. 8E) staining results. In conclusion, HIDs hydrogel is beneficial to repair wound healing and accelerate skin regeneration.

4. Conclusions

To enhance the efficiency and comfort of clinical wound treatment, we have successfully manufactured a functional hydrogel with controllable adhesion. This achievement was made possible through the incorporation of dopamine and imidazole derivatives, along with the strategic use of metal ions. This formulation significantly enhances the antibacterial and adhesive properties of the dressing, contributing to the overall improvement of wound healing processes. The dressing, designed to work synergistically with various metal ions, controllably regulates the adhesion and detachment, optimizing the healing environment.

The hydroxyl group of dopamine, combined with the interface adhesion effect achieved through topological entanglement, imparts strong adhesion capabilities to HIDs hydrogels. The adhesion strength to pig skin reaches an impressive 6 kPa, ensuring stable adherence to wound tissue. Furthermore, the imidazole derivatives play a crucial role in inhibiting the growth and reproduction of diverse bacteria within wounds, creating a physiologically conducive environment for wound repair.

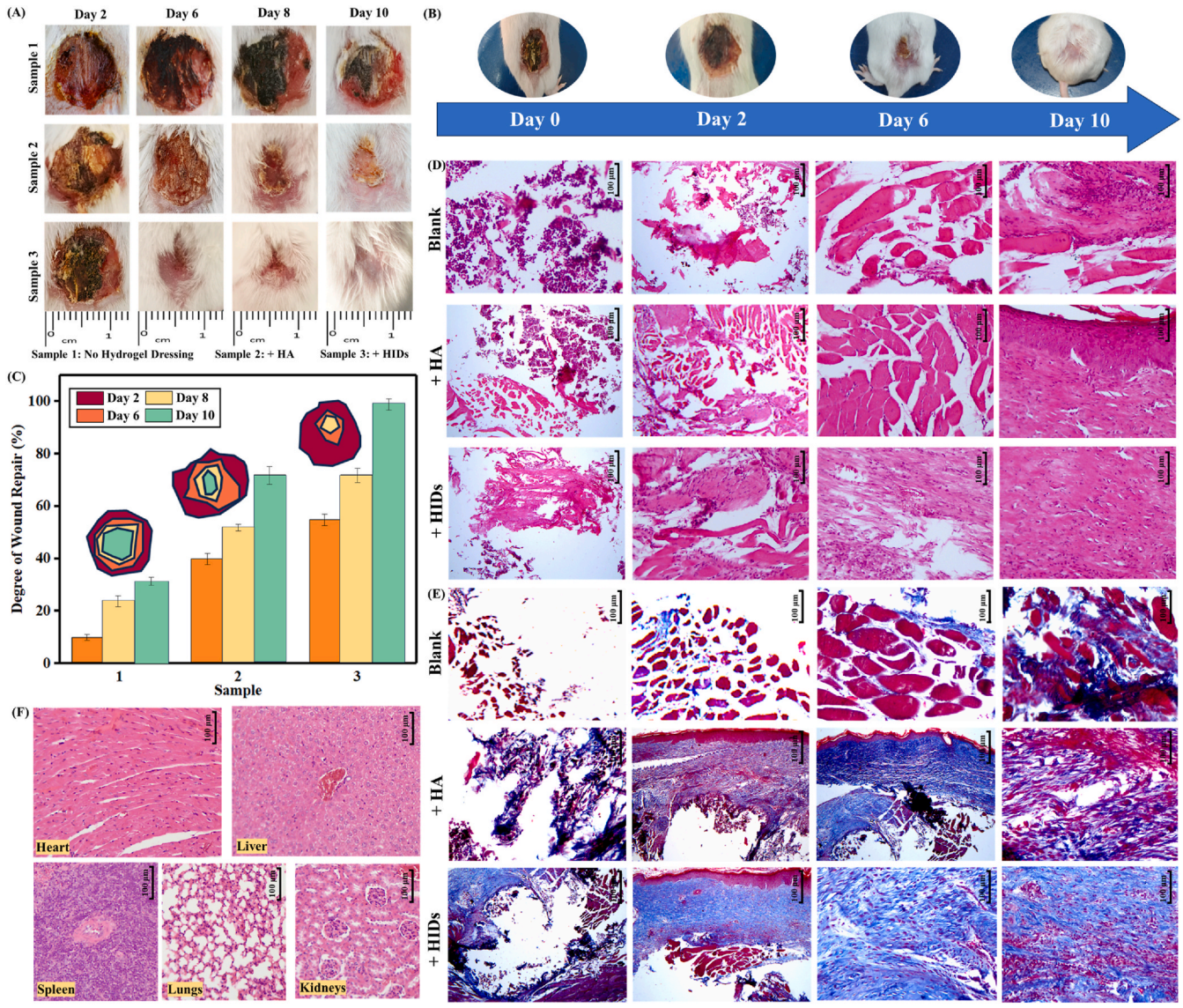

Fig. 8. Testing the effect of HIDs on wound healing. **(A)** The photographs of wound healing. **(B)** Schematic diagram of wound healing in mice. (n = 15) **(C)** Mouse wound change model and healing data. **(D)** Remove the surrounding tissue of the defect and evaluate it using H&E staining on days 2, 4, 6, and 10. (n = 3) **(E)** The tissue around the defect was excised and Masson trichrome staining was used to evaluate the wound healing of HIDs hydrogel on the 2nd, 4th, 6th and 10th days. (n = 3) **(F)** Organs of mice cured by HIDs will be sliced and analyzed histologically. (From left to right are the heart, liver, spleen, lungs, and kidneys in order).

Table 2
The surface area of wound during healing process.

Group	Time	Area (cm^2)	Area (cm^2)	Area (cm^2)	Area (cm^2)
Control Group	**Day 0**	1.692	1.623	1.687	1.653
	Day 2	1.557	1.488	1.547	1.527
	Day 6	1.523	1.428	1.518	1.504
	Day 8	1.308	1.246	1.301	1.268
	Day 10	1.169	1.112	1.171	1.150
HA	**Day 0**	1.693	1.634	1.693	1.659
	Day 2	1.106	1.059	1.095	1.087
	Day 6	1.019	0.998	1.026	0.990
	Day 8	0.802	0.766	0.819	0.801
	Day 10	0.489	0.452	0.457	0.471
HIDs	**Day 0**	1.640	1.645	1.687	1.699
	Day 2	1.002	0.966	0.995	0.982
	Day 6	0.764	0.734	0.764	0.742
	Day 8	0.478	0.456	0.467	0.478
	Day 10	0	0	0.017	0.017

In summary, our study demonstrates the practical utility of HIDs hydrogel dressing in actively promoting the healing of comprehensive cortical wounds through the utilization of different metal ions. Such advancements make this dressing highly valuable and marketable in the realm of wound care.

CRediT authorship contribution statement

Zihao Shen: Writing – original draft, Visualization, Methodology, Conceptualization. **Ningyi Ma:** Writing – original draft, Software, Investigation. **Juan Xu:** Writing – review & editing, Validation, Supervision, Conceptualization. **Ting Wang:** Writing – review & editing, Supervision, Conceptualization.

Declaration of competing interest

The authors declare that they have no known competing financial interests or personal relationships that could have appeared to influence the work reported in this paper.

Data availability

No data was used for the research described in the article.

Acknowledgment

All authors thank the supporting of the Non-profit Central Research Institute Fund of National Research Institute for Family Planning (2022GJZ06).

References

[1] GBD 2019 Antimicrobial Resistance Collaborators, Global mortality associated with 33 bacterial pathogens in 2019: a systematic analysis for the global burden of disease study 2019, Lancet 400 (2022) 2221–2248.
[2] N. Kucisec-Tepes, D. Bejuk, D. Kosuta, [Characteristics of war wound infection], Acta Med. Croat. 60 (2006) 353–363.
[3] D. Church, S. Elsayed, O. Reid, B. Winston, R. Lindsay, Burn wound infections. Clin, Nat. Rev. Microbiol. 19 (2006) 403–434.
[4] Y. Wu, Y. Wang, L. Long, C. Hu, Q. Kong, Y. Wang, A spatiotemporal release platform based on pH/ROS stimuli-responsive hydrogel in wound repairing, J. Contr. Release 341 (2022) 147–165.
[5] T. Ohura, T. Nakajo, S. Okada, K. Omura, K. Adachi, Evaluation of effects of nutrition intervention on healing of pressure ulcers and nutritional states (randomized controlled trial), Wound Repair Regen. 19 (2011) 330–336.
[6] Y. Lu, H. Li, J. Wang, M. Yao, Y. Peng, T. Liu, Z. Li, G. Luo, J. Deng, Engineering bacteria-activated multifunctionalized hydrogel for promoting diabetic wound healing, Adv. Funct. Mater. 31 (2021) 2105749.
[7] H.M. Nguyen, T.T.N. Le, A.T. Nguyen, H.N.T. Le, T.T. Pham, Biomedical materials for wound dressing: recent advances and applications, RSC Adv. 13 (2023) 5509–5528.
[8] S.-W. Huang, Y.-F. Wu, T. Ahmed, S.-C. Pan, C.-M. Cheng, Point-of-care detection devices for wound care and monitoring, Trends Biotechnol. 42 (2023) 74–90.
[9] C.K. Sen, Human wounds and its burden: an updated compendium of estimates, Adv. Wound Care 8 (2019) 39–48.
[10] Emergency Preparedness, Prevention and management of wound infection, WPE (2013). https://www.who.int/publications/i/item/prevention-and-management-of-wound-infection.
[11] M.Y. Zheng, Realizing a major innovation in the concept of wound repair in China with the goal of shortening wound healing time and improving healing quality——"Key technologies and applications of biomaterials in wound repair microenvironment", first prize of the 2020 Chinese Medical Science and Technology Award for Medical Science and Technology, China Med. News 36 (2021) 15, 15.
[12] D.H. Hu, K. Tao, [Lay emphasis on the basic research in the field of burn surgery in China], Chin. J. Burns Wounds 32 (2016) 385–388.
[13] Y. Yang, Y. Ma, J. Wang, L. You, R. Zhang, Q. Meng, S. Zhong, W. He, X. Cui, Chitosan-based mussel-inspired hydrogel for rapid self-healing and high adhesion of tissue adhesion and wound dressings, Carbohydr. Polym. 316 (2023) 121083.
[14] T.-W. Chung, C.-L. Cheng, Y.-H. Liu, Y.-C. Huang, W.-P. Chen, A.K. Panda, W.-L. Chen, Dopamine-dependent functions of hyaluronic acid/dopamine/silk fibroin hydrogels that highly enhance N-acetyl-L-cysteine (NAC) delivered from nasal cavity to brain tissue through a near-infrared photothermal effect on the NAC-loaded hydrogels, Biotechnol. Adv. 154 (2023) 213615.
[15] S.Y. Zheng, S. Mao, J. Yuan, S. Wang, X. He, X. Zhang, C. Du, D. Zhang, Z.L. Wu, J. Yang, Molecularly engineered zwitterionic hydrogels with high toughness and self-healing capacity for soft electronics applications, Chem. Mater. 33 (2021) 8418–8429.
[16] Z. Shen, C. Zhang, T. Wang, J. Xu, Advances in functional hydrogel wound dressings: a review, Polymers 15 (2023) 2000.
[17] M. Deptuła, M. Zawrzykraj, J. Sawicka, A. Banach-Kopeć, R. Tylingo, M. Pikuła, Application of 3D- printed hydrogels in wound healing and regenerative medicine, Biomed. Pharmacother. 167 (2023) 115416.
[18] B. Guo, R. Dong, Y. Liang, M. Li, Haemostatic materials for wound healing applications, Nat. Rev. Chem 5 (2021) 773–791.
[19] Y. Xu, B. Wang, D. Peng, X. Nie, J. Wang, C.-Y. Yu, H. Wei, Hyaluronic acid-based injectable hydrogels for wound dressing and localized tumor therapy: a review, Adv. NanoBiomed Res. 2 (2022) 2200124, 2200124.
[20] I.L. Mohd Isa, S.A. Abbah, M. Kilcoyne, D. Sakai, P. Dockery, D.P. Finn, A. Pandit, Implantation of hyaluronic acid hydrogel prevents the pain phenotype in a rat model of intervertebral disc injury, Sci. Adv. 4 (2018) 2375–2548.
[21] G.Ş. Andrei, B.F. Andrei, P.R. Roxana, Imidazole derivatives and their antibacterial activity – a mini-review, Mini-Rev. Med. Chem. 21 (2021) 1380–1392.
[22] Y. Li, P. Yu, J. Wen, H. Sun, D. Wang, J. Liu, J. Li, H. Chu, Nanozyme-based stretchable hydrogel of low hysteresis with antibacterial and antioxidant dual functions for closely fitting and wound healing in movable parts, Adv. Funct. Mater. 32 (2021) 2110720.
[23] Q. Yan, L.L. Liu, T. Wang, H.N. Wang, A pH-responsive hydrogel system based on cellulose and dopamine with controlled hydrophobic drug delivery ability and long-term bacteriostatic property, Colloid Polym. Sci. 297 (2019) 705–717.
[24] Y. Li, R. Fu, Z. Duan, C. Zhu, D. Fan, Artificial nonenzymatic antioxidant MXene nanosheet-anchored injectable hydrogel as a mild photothermal-controlled oxygen release platform for diabetic wound healing, ACS Nano 16 (2022) 7486–7502.
[25] P.-Y. Wang, M.-W. Wang, D. Zeng, M. Xiang, J.-R. Rao, Q.-Q. Liu, L.-W. Liu, Z.-B. Wu, Z. Li, B.-A. Song, S. Yang, Rational optimization and action mechanism of novel imidazole (or imidazolium)-labeled 1,3,4-oxadiazole thioethers as promising antibacterial agents against plant bacterial diseases, J. Agric. Food Chem. 67 (2019) 3535–3545.
[26] H. Zhang, X. Sun, J. Wang, Y. Zhang, M. Dong, T. Bu, L. Li, Y. Liu, L. Wang, Multifunctional injectable hydrogel dressings for effectively accelerating wound healing: enhancing biomineralization strategy, Adv. Funct. Mater. 31 (2021) 2100093.
[27] A. Jastram, J. Claus, P.A. Janmey, U. Kragl, Rheological properties of hydrogels based on ionic liquids, Polym. Test. 93 (2021) 106943.
[28] X.X. Lin, X.L. Wang, L.P. Zeng, Z.L. Wu, H. Guo, D. Hourdet, Stimuli-Responsive toughening of hydrogels, Chem. Mater. 33 (2021) 7633–7656.
[29] K. Zhang, Q. Feng, Z. Fang, L. Gu, L. Bian, Structurally dynamic hydrogels for biomedical applications: pursuing a fine balance between macroscopic stability and microscopic dynamics, Chem. Rev. 121 (2021) 11149–11193.
[30] Y. Hua, Y. Gan, Y. Zhang, B. Ouyang, B. Tu, C. Zhang, X. Zhong, C. Bao, Y. Yang, Q. Lin, Q. Zhou, L. Zhu, Adaptable to mechanically stable hydrogels based on the dynamic covalent cross-linking of thiol-aldehyde addition, ACS Macro Lett. 8 (2019) 310–314.
[31] H. Ren, Z. Zhang, X. Cheng, Z. Zou, X. Chen, C. He, Injectable, self-healing hydrogel adhesives with firm tissue adhesion and on-demand biodegradation for sutureless wound closure, Sci. Adv. 9 (2023) eadh4327.
[32] Y. Qiao, J. He, W. Chen, Y. Yu, W. Li, Z. Du, T. Xie, Y. Ye, S.Y. Hua, D. Zhong, K. Yao, M. Zhou, Light-activatable synergistic therapy of drug-resistant bacteria-infected cutaneous chronic wounds and nonhealing keratitis by cupriferous hollow nanoshells, ACS Nano 14 (2020) 3299–3315.
[33] FAO/WHO Codex Alimentarius Commission & Joint FAO/WHO Food Standards Programme, Food labelling: complete texts, 2001 rev, Food and Agriculture Organization of the United Nations (2001). https://iris.who.int/handle/10665/42477.
[34] S.C. Walpole, D. Prieto-Merino, P. Edwards, J. Cleland, G. Stevens, I. Roberts, The weight of nations: an estimation of adult human biomass, BMC Publ. Health 18 (2012) 439.
[35] J. Hu, D. Liu, On metal coordination ability, J. Hanjiang Normal Univ. 30 (2010) 2.
[36] B. Hosseinzadeh, M. Ahmadi, Degradable hydrogels: design mechanisms and versatile applications, Mater. Today Sustain. 23 (2023) 100468.
[37] B.G. Yang, K.C. Wei, C. Loebel, K.Y. Zhang, Q. Feng, R. Li, S.H.D. Wong, X.Y. Xu, C. H. Lau, X.Y. Chen, P.C. Zhao, C. Yin, J.A. Burdick, Y. Wang, L.M. Bian, Enhanced mechanosensing of cells in synthetic 3D matrix with controlled biophysical dynamics, Nat. Commun. 12 (2021) 3514.
[38] W. Shi, D. Zhang, L. Han, W. Shao, Q. Liu, B. Song, G. Yan, R. Tang, X. Yang, Supramolecular chitin-based hydrogels with self-adapting and fast-degradation properties for enhancing wound healing, Carbohydr. Polym. 323 (2024) 121374.
[39] R. Yang, X. Liu, Y. Ren, W. Xue, S. Liu, P. Wang, M. Zhao, H. Xu, B. Chi, Injectable adaptive self-healing hyaluronic acid/poly (γ-glutamic acid) hydrogel for cutaneous wound healing, Acta Biomater. 127 (2021) 102–115.
[40] D. Duquette, M.J. Dumont, Comparative studies of chemical crosslinking reactions and applications of bio-based hydrogels, Polym. Bull. 76 (2019) 2683–2710.
[41] N. Rani, P. Kumar, R. Singh, Molecular modeling studies of halogenated imidazoles against 14α-demethylase from Candida albicans for treating fungal infections, Infect. Disord.: Drug Targets 20 (2020) 208–222.
[42] National Health Commission of the PRC, Management specification for disinfection product label instructions, NHC (2005). http://www.nhc.gov.cn/bgt/pw10511/200603/073542f7aa774d3ca4ec368cd35961f1.shtml).
[43] National Health Commission of the PRC, Technical specification on antimicrobial susceptibility tests, NHC (2018). http://www.nhc.gov.cn/old_file/uploadfile/20190107102217856.pdf.
[44] ISO, Biological evaluation of medical devices — Part 5: tests for in vitro cytotoxicity, ISO/TC 194 (2009). https://std.samr.gov.cn/gj/search/gjDetailed?id=2813DFD07006C59719C53F82452BB1B4.
[45] M. Dovedytis, Z. Liu, S. Bartlett, Hyaluronic acid and its biomedical applications: a review, Eng. Regen. 1 (2020) 102–113.
[46] M. Litwiniuk, A. Krejner, M. Speyrer, A. Gauto, T. Grzela, Hyaluronic acid in inflammation and tissue regeneration, Wounds 28 (2016) 78–88.
[47] A.H. Fischer, K.A. Jacobson, J. Rose, R. Zeller, Hematoxylin and eosin staining of tissue and cell sections, Cold Spring Harb. Protoc. 2008 (2008). , pdb.prot4986.
[48] A. Ozawa, M. Sakaue, New decolorization method produces more information from tissue sections stained with hematoxylin and eosin stain and Masson-trichrome stain, Ann. Anatomy - Anatomischer Anzeiger 227 (2020) 151431.